Contribution of GIS and remote sensing in geological mapping, lineament extractions and hydrothermal alteration minerals mapping using ASTER satellite images: case study of central Jebilets - Morocco

Farah Abdelouhed*, Ahmed Algouti, Abdellah Algouti, Ifkirne Mohammed and Zahra Mourabit
Department of Geology, Cadi Ayyad University Marrakech, MOROCCO
*Farah6farah@gmail.com

Abstract
The Jebilet massif is part of the Paleozoic Hercynian chain located in the western meseta of Morocco. It conceals several polymetallic mines and several mining indices (Copper, Lead and Zinc). The most important mines such as Draa Sfar, Koudiat Aicha, Laachach, Bir Enhass and Kettara. Mineralisation are attributed to Volcanic Massive Sulphide (VMS) types. These types of genetic model are accompanied by hydrothermal alteration with a very particular mapping zonation of minerals alteration. These minerals including chlorite, sericite, illite as well as iron oxides are accompanying mineralization in the majority of cases.

To understand the contribution of Geographic Information System (GIS) and remote sensing for mapping the spatial distribution of hydrothermal alteration minerals, geological mapping, lineament extraction (structural) at the Central Jebilet scale, we used GIS and satellite image processing software ArcGIS and ENVI, PC Geomatica 2016. The ENVI software allowed us to extract the alteration minerals namely the silicate group by band ratio. The methods of supervised classification showed us that basic magmatic bodies from the North East are acidic bodies following the application of the Spectral Angle Mapper (SAM) classification which is based on the spectral signatures of the samples. PC Géomatica 2016 has also allowed the extraction of lineaments in the study area following treatments carried out on the digital field model STRM with a spatial resolution of 30 meter. In addition, the ArcGIS software was used to georeference and overlap data from different sources and to lay out the maps. The mapping results obtained by GIS and remote sensing provide an input to the exploitation in the central jbilets. They could also provide metallotects for the exploration of similar deposits in the metallogenic province of Jebilets Guemassa.

Keywords: GIS, Aster, Central jebilets, Geological mapping, Lineaments maps, Hydrothermal alteration.

Introduction

In spite of the importance of the earlier works reported on the central jebilets sector, some aspects of the geological, structural and hydrothermal alteration mapping would deserve for improvement of the potential of mineral resources.

Indeed, in order to know the details of the geological and structural context of this targeted zone, the objective of this study is to highlight the effectiveness of images in lithological, structural and hydrothermal alteration mapping. The Hercynian massif of Jebilet-Gemassa is a metallogenic sulphide province with pyrrhotite dominance[3,4,11,12,15] Sarhlef series that covers most of the Central Jebilets. This series is composed of a sandstone and pelitic sedimentary sequence[5] with intercalations of acidic and basic volcanic along with volcano sedimentary rocks.[1,9,10]

Geographic setting: Geographically the Central jebilet Hercynian Massif forms are part of the southern Moroccan Meseta[16]. This massif consists of a set of hills and rocky plains extending from the north of Marrakesh in an E-W direction over an area of about 3,800 km² between longitudes 7°W and 8°50'W and latitudes 31°45'N and 32°05'N , The Central Jebilet Massif is limited to the north by the Bahira plain, to the south by the Haouz plain, to the east by the the Oriental Jebilets and to the west by the Jurassic-Cretaceous terrain of the Mouissate (Figure 1).

Geological setting: The lithology of the area is dominated by pelites constituting the major facies of the central jebilets which are distributed from the west to east by greenish to greyish silicified pelites. They are generally chloritized and hematitized showing calcareous centimetric intercalations and sericitized black pelites. To the east and south-east of the sector, there are rather mafic units that have been described as microgabbro and microdiorite[7].

Large white quartz veins in the N30 direction of metric power outcrop all along the iron cap from South to North. They are generally intersected by the general N115 direction faults and dexter and sinister shears that have affected the zone. The iron cap (Figure 2) itself shows a N-S direction which becomes N030 towards the north in the vicinity of the Mesert fault of the general East-West direction.

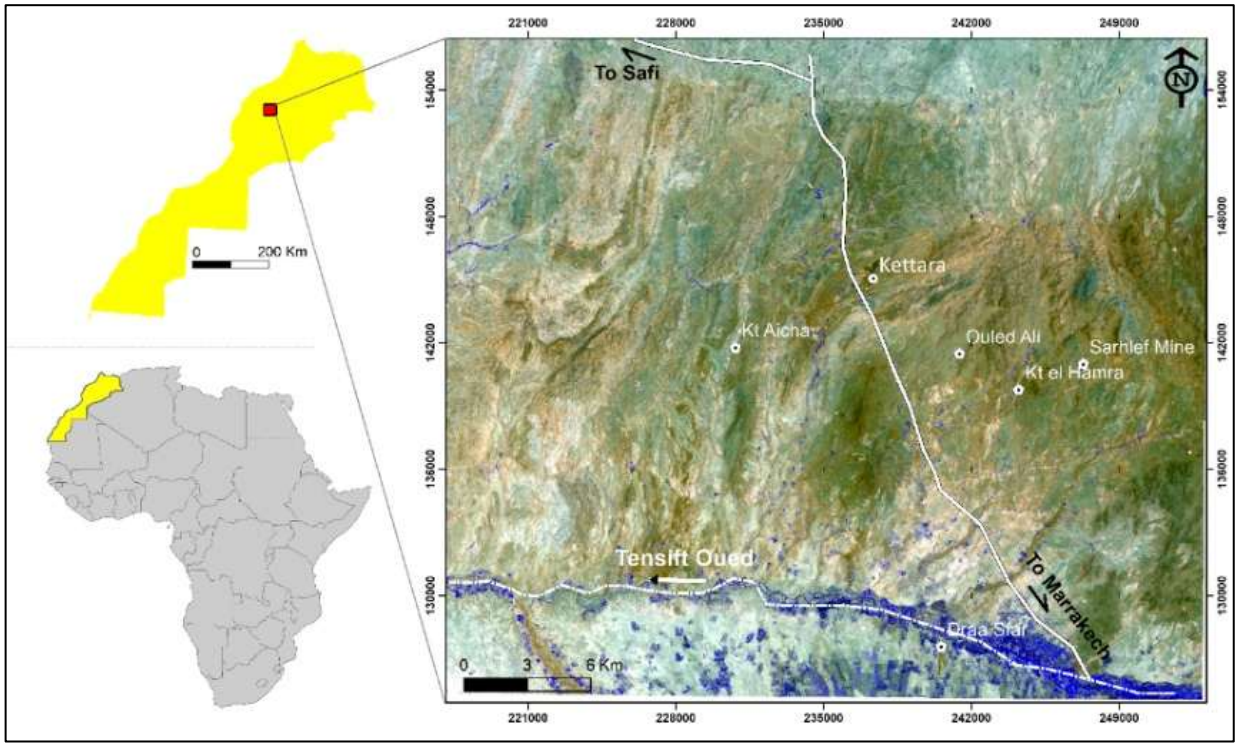

Fig. 1: ASTER image (1, 2, 3) in RGB showing the location of the study area "Hercynian outcrops of the Jebilets-Guemassa, with the location of the main deposits of sulphide deposits modified[12]

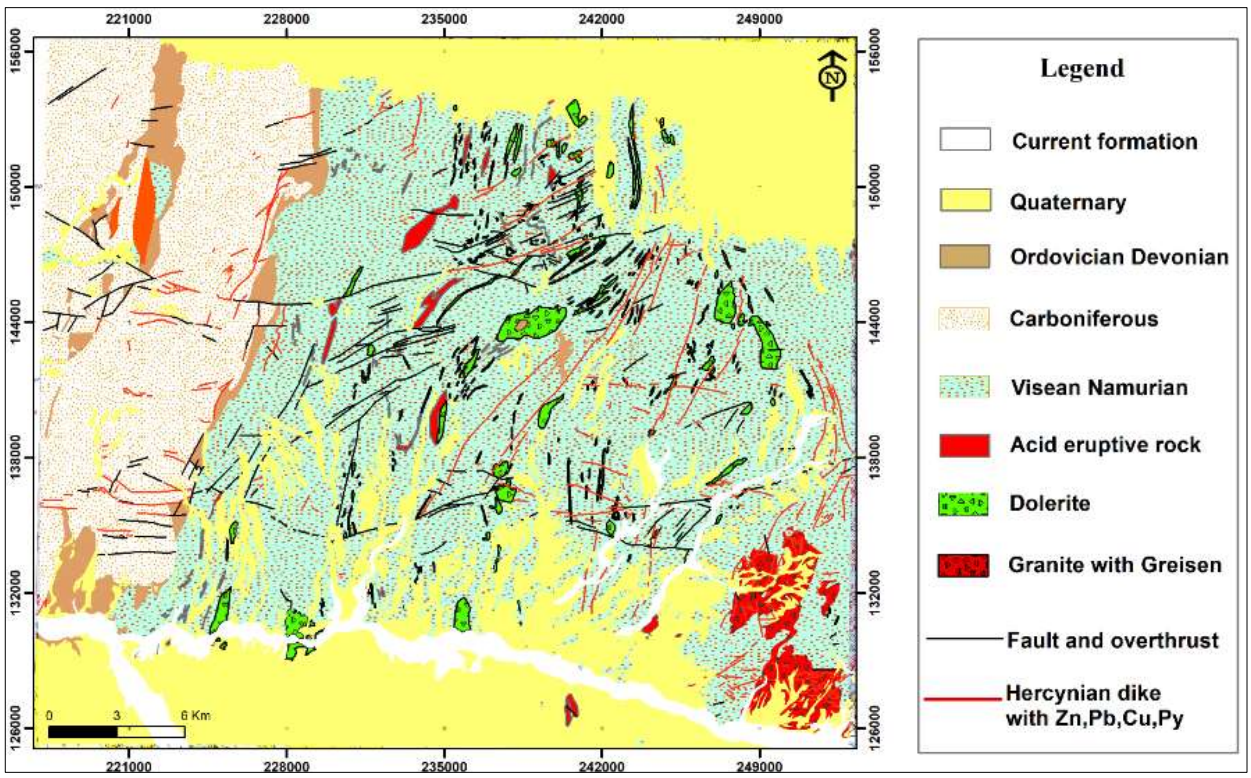

Fig. 2: Simplified geological map of central Jebilet and deposit locations and massive sulphide indexes[12]

Material and Methods

The Advanced Spaceborne Thermal Emission and Reflection Radiometer (ASTER) is essentially a large digital camera that captures images in the visible and infrared. Since 1999, this experimental sensor has been orbiting the earth aboard NASA's Terra satellite. Terra was launched in December 1999 as part of the Earth Observation System. A collaborative initiative between the United States and Japan, ASTER has covered the entire surface of the Earth at least once to date. Since each image captured covers an area of 60 X 60 km, ASTER is used to obtain a detailed information

about the Earth's surface including temperature, emissivity, reflectance, elevation and geology.

ASTER collects high spatial resolution data in 14 bands with wavelengths ranging from the visible to the thermal infrared (Figure 3). It can provide stereograms for the creation of digital elevation models. It is mainly used for detailed regional environmental monitoring and mapping exercises. Imagery for an area of interest is available on a weekly basis depending on cloud covers. One of the most important features of ASTER is its high resolution, with a pixel size of 15 m in bands 1 to 3 (compared to the 15 to 30 m resolution of the Landsat TM sensor).

The high resolution is useful to resource managers since a more detailed image makes it easier to detect changes in land use. Eleven additional bands cover regions of the spectrum in the shortwave infrared (SWIR) and thermal infrared (TI) radiations. The swath width of the IRCL and RIT sensors is 60 km and their spatial resolution is 30 m and 90 m respectively. This stereoscopic capability makes ASTER ideal for geological and geomorphological interpretations.[2]

Methodology

This work was carried out using ENVI 5.3, QGIS, PC GEOMATICA 2016, ArcGIS 10.5 and consists of respecting the spatial conformity of the data, particularly with regard to future image corrections and layer stacking and pan-sharpening. The image used in this work is an ASTER type image resulting from radiometric calibration, atmospheric corrections, geometric corrections of the raw image and then a filling of the VNIR and SWIR bands (layer-stacking) followed by pan-sharpening with Landsat 8 panchromatic image of the same area (figure 4).

Subsystem	Band No.	Spectral Range (μm)	Spatial Resolution, m	Quantization Levels
VNIR	1	0.52-0.60	15	8 bits
	2	0.63-0.69		
	3N	0.78-0.86		
	3B	0.78-0.86		
SWIR	4	1.60-1.70	30	8 bits
	5	2.145-2.185		
	6	2.185-2.225		
	7	2.235-2.285		
	8	2.295-2.365		
	9	2.360-2.430		
TIR	10	8.125-8.475	90	12 bits
	11	8.475-8.825		
	12	8.925-9.275		
	13	10.25-10.95		
	14	10.95-11.65		

Fig. 3: ASTER satellite sensor specifications. (NASA 2004)

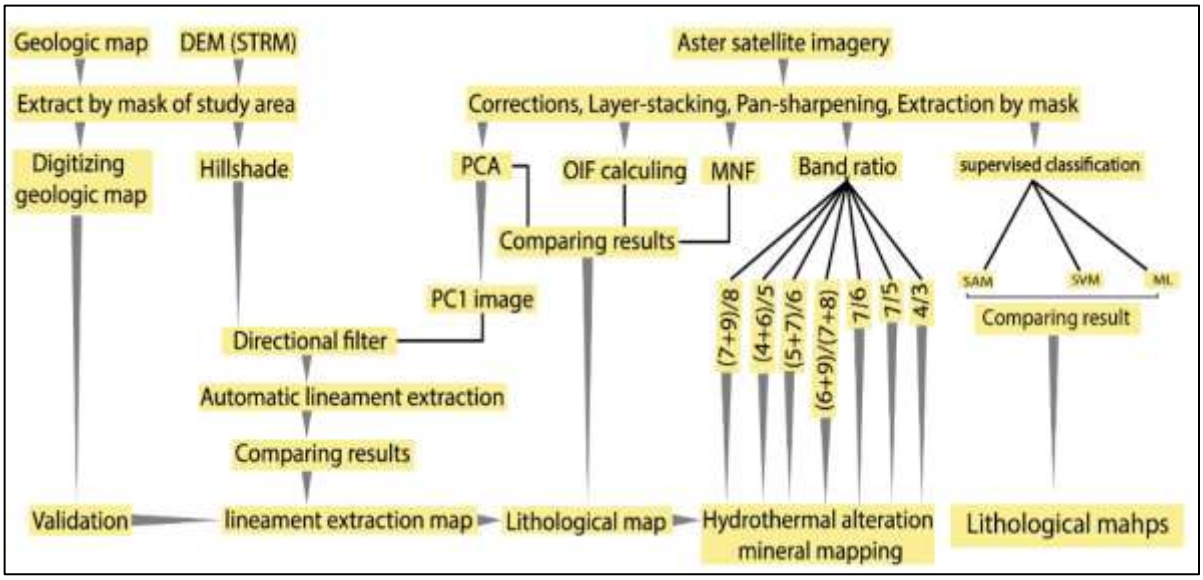

Fig. 4: Flowchart for lithological, lineaments and hydrothermal alteration mapping of minerals in the central jebilets region based on Aster data

Results and Discussion

Lithological mapping

a. Principal Component Analysis: One of the techniques used to create the new channels is Principal Component Analysis (PCA). This technique is widely used in remote sensing to condense the information distributed over the many spectral bands of our Aster scene. The new components of this technique typically represent up to 97% of the original or initial data set. After calculation of the PCA nanochannel's, it appears that the colorimetric composition (CP1, CP2, CP4) RGB (Figure 5A) generated from 9 ASTER bands is the best for lithological interpretation. We then decided to use the first three components providing a clear color composition which allows the discrimination of the different lithological units. By applying treatments to this ACP technique, we have distinguished the following training courses, concerning the colored compound map (Figure 5A).

First lithological discrimination which has a mixed hue of (pink, blue and green) for Ordovician to Devonian (O-D) age terrains outcrops in the N-W part. Second lithological discrimination has a green hue characterizing the current formations (A) generally located in the southern part of the map and around Wadi Tensift.

In addition a third lithological discrimination in red tint determines the lithological formation of Plio-Villafranchien which is concentrated in the S-W part of the map but some outcrops in the N-E are well distinguished. This is the case for the grey image CP1 (Figure 5 B), The O-D age terrains are well discriminated by a mosaic-white tint while the Plio-Villafranchian lithological formations are also discriminated by an off-white tint.

b. Optimum Index Factor (OIF) and Minimum Noise Fraction (MNF): For a truly quantitative selection of the best band combinations for extracting the maximum amount of information[7], the notion of the "Optimum Index Factor" was introduced where OIF is calculated as ka:

$$(OIF) = \frac{\sum_{K=1}^{3} SK}{\sum_{j=1}^{3} |r\,j|} \qquad (1)$$

where Σ Sk = Sum of the standard deviations (s.d) of the combinations of the 3 bands k1, k 2, k 3. Σ IrjI = Sum of the absolute values of the correlation coefficient. Another transformation technique can be applied, the Minimum Noise Fraction (MNF), which is an analysis treatment that shows the variation between bands in an image and identifies the location of spectral anomalies. Rotational MNF transformations are used to determine the inherent dimensionality of image data, to separate noise in the data and to reduce computational requirements for further processing[6].

Figure 6 on the right shows the false color compound 124 of the OIF calculation result, where band 1, band 2 and band 4 corresponds to VNIR1 VNIR2 and SWIR1 respectively. On the right, it shows the result of the MNF transformation. This method is similar to PCA and it is used as a preparatory transformation to condense the main components in a controlled number of spectral bands.

The first MNF bands contain signals and the remaining bands contain noise. The O-D formations appear in red in the OIF map while the Plio-Villafranchian (qa) formations appear in well-distinguished pink; also the discrimination of the current formations (A) is clearly visible on both the OIF and MNF maps (Figure 6). The treatments in colored compositions, MNF, OIF and ACP, allowed us a very good discrimination of the lithologies encountered in our zone of study. The different training courses can be clearly individualized.

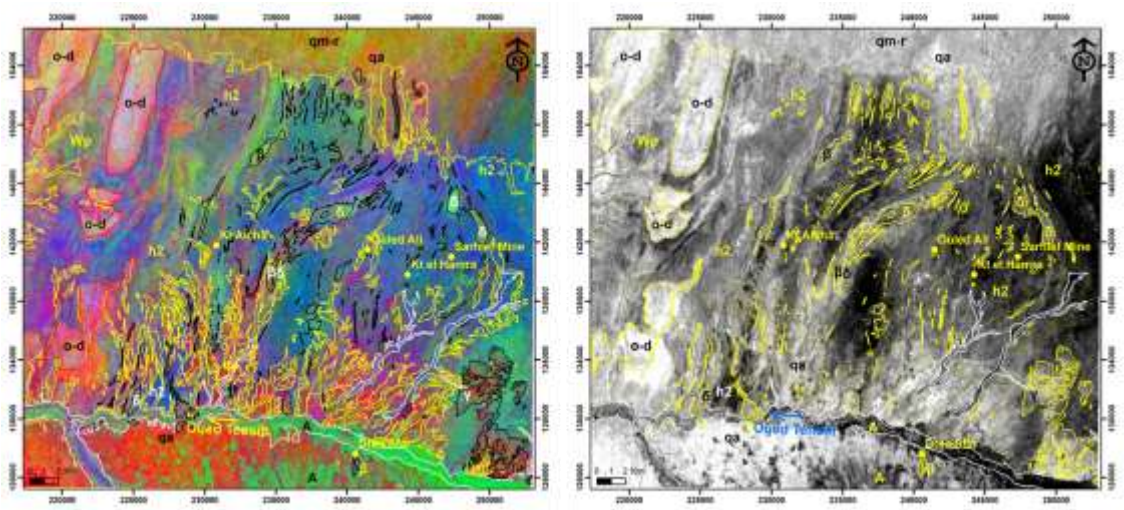

Fig. 5: In the left RGB colored compound of the PC images (CP1, CP2, CP4) and in gray level on the right the CP1 image of the study area, (O-D):Ordovician to Devonian,h2:upper target, qa: Plio-Villafranchian, qm-r: Middle Pleistocene to recent, Wp: Westphalo-Permian, A: current formation,β:basic intrusion, δ:acidic intrusion)

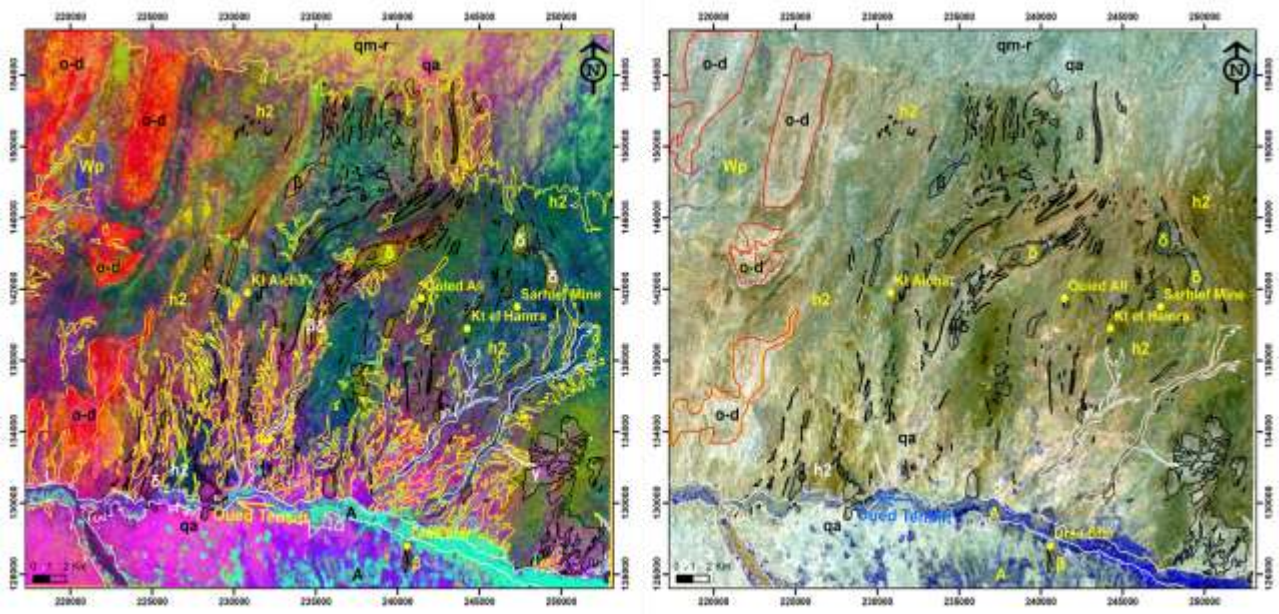

Fig. 6: Map of the best RGB combination of the spectral bands of the ASTER image on the basis of the OIF calculation(right) with the result of the MNF transformation on the left (O-D):Ordovician to Devonian,(h2):upper target, qa: Plio-Villafranchian, qm-r: Middle Pleistocene to recent, Wp: Westphalo-Permian, A: current formation,β:basic intrusion, δ:acidic intrusion)

c. Scupervised classification: It is strongly recommended to apply the supervised classification technique in this work to better understand all the facies that make up our study area. The classification was carried out using a region of interest and spectral signatures.

Maximum Likelihood (ML): This classification assumes that the statistics for each class in each band were normally distributed and to calculate the probability that a given pixel belongs to a specific class. Unless a probability threshold, all pixels were classified. Each pixel was assigned to the class that has the highest probability (that is, the maximum likelihood). If the highest probability is smaller than a threshold, we specify the pixel remains as unclassified. ENVI and implements maximum likelihood classification by calculating the following discriminate functions for each pixel in the image[17]:

$$g_i(x) = lnp(w_i) - {}^1/_2\ ln\left|\sum_i\right| - {}^1/_2\ (x-m_i)^t \sum_i^{-1} (x-m_i)$$

where i = class; x = n-dimensional data (where n is the number of bands); p (ωi) = probability that class ωi occurs in the image and is assumed the same for all classes; |Σi| = determinant of the covariance matrix of the data in class ωi; Σi-1 = its inverse matrix; mi = mean vector .In the present study, maximum likelihoods were applied on the aster bands in the study area using (ROIs)) with overall accuracy 95.0 % (Figure 7A).

Spectral Angle Mapper (SAM): The SAM method produces a classified image based on the specified value for the maximum SAM angle. Lowering this threshold usually results in fewer corresponding pixels (better match with the reference spectrum). While increasing this threshold may result in a more spatially consistent image. However, the matches between pixels will not be as good as for the lower threshold. This technique has been applied to the ASTER bands in the study area using (spectral signatures) with overall accuracy with 92% (Figure 7 B).

From the confusion matrices (Overall accuracy and Kappa index),it can be noted that the maximum likelihood (ML) and spectral angle mapper classification give good results based on Kappa index values of 0.92 for SAM and 0.95 for M.Th. Supervised classification has well discriminated the geological formations at the level of the Central Jebilets. More than that, other formations have been observed and which did not exist on the geological map of 1/100000 namely the NNW carbonate formations of the Central Jebilets of Ordovician Devonian age, acidic and basic magmatic bodies at the base of their spectral signatures.

On the other hand, the SAM type classification based on the spectral signatures of the studied facies showed a contradiction between the magmatic bodies between what was in the geological map and what was found during the classification, Originally basic magmatic bodies were classified in the category of acidic magmatic bodies after the classification, which is not foreseen. The classification of other acidic-basic magmatic bodies, also their alteration is seen in Board 2 in appendices figures A, B, C, D, E, F, G and H.

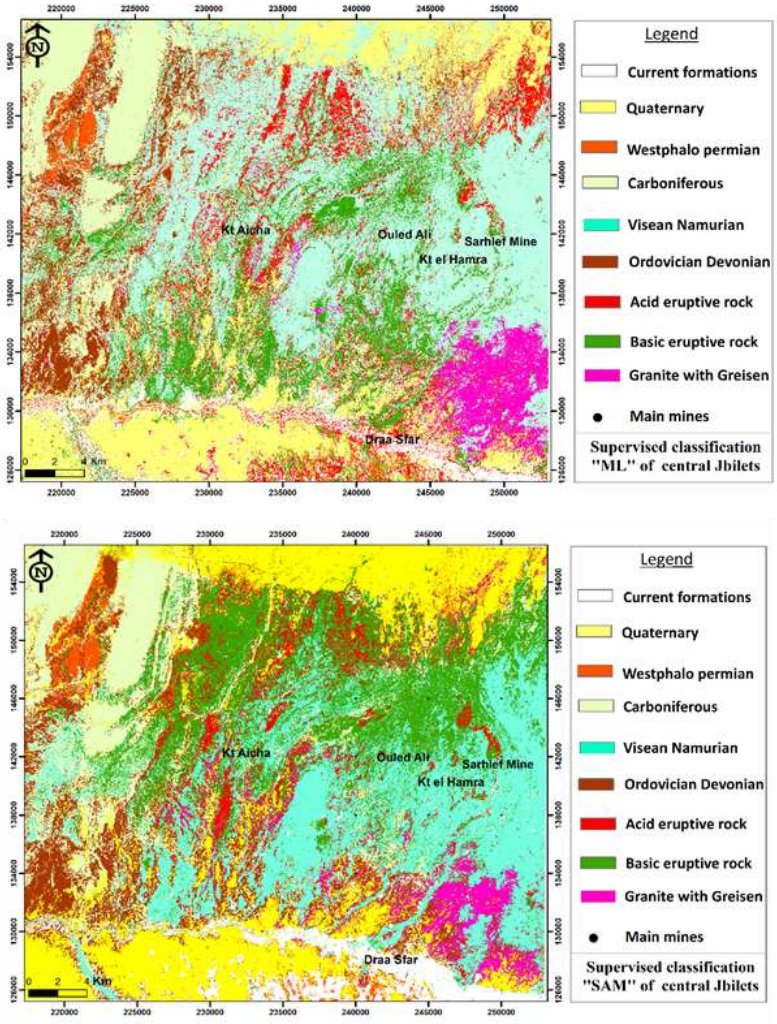

Fig. 7: Lithological map of Maximum likelihood classification using ROIs for the Jebilets Central and Lithological map of Spectral Angle Mapper (SAM) for the Jebilets Central

Extraction of lineaments: In the Central Jebilets, the Carboniferous terrains (Sarhlef shales) are affected by an intense Hercynian deformation characterized by a complex tectometamorphic history. First, they underwent a phase of synschist folding in a submeridian direction associated with a zonal epic metamorphism of the upper post-visual age[13]. Then, they were affected by sub-parallel shearing to the flow schistosity. This associated with this general metamorphism is a periplutonic metamorphism that develops around granitic (Board 1 in appendices, Figure C) and gabbroic (Board 1 in appendices, Figure F) intrusions with halos of metamorphism. sinister N160° dips and large submeridian faults associated with the Stephano-permian trenches.

After the pre-processing of the ASTER image (corrections, band stacking, pan-sharpening, mask extraction, PCA) and of the Digital Terrain Module (mosaic, area extraction, shading), directional filters matrix(3X3) can be applied to the different neochannels in order to generate lineaments map and their analyses. The methods used to extract lineaments are convolution methods. This is the Sobel filter used to detect the contours of objects in an image by making two horizontal and vertical scans, It often gives good results for the detection of lineaments and directional filters that improve the perception of lineaments corresponding to lithological or structural discontinuities by causing an optical effect of cast shadow on the image.

The maps in the figures show the results of lineament extraction after making all necessary corrections detailed in the methodology (Figure 4). For the map of the extracted lineaments using the CP1 band, (Figure 8B), in order to better map all the tectonic aspects affecting the area we applied directional filters to the matrix (3X 3), defining the angles ('0°,45°;90° and 135°), after having represented all the faults extracted on a directional rosette. The realization of a density map of CP 1 lineaments (Figure 9B) is well recommended to locate points where tectonic activity is intensifying. For the second lineament map made DTM map (Figure 8C) we also applied directional filters matrix (3 X 3) and defining the angles('0°, 45°, 90° and 135°) and the results were represented in directional rosettes, thus making a lineament intensity map (Figure 9C).

On the basis of these two maps we concluded that lineament mapping using aster images is a powerful tool to be used

especially in the tectonic characterization of the sector, in particular as the faults control the mineralization of central jebilts. The field missions carried out (plate) allowed us to validate some data (several measurements of faults in K. AICHA. lAACHACH, also the validation of the nature of certain facies and iron cap with the index minerals and other aspects of alteration can be a very good guide for mineral prospecting in the future).

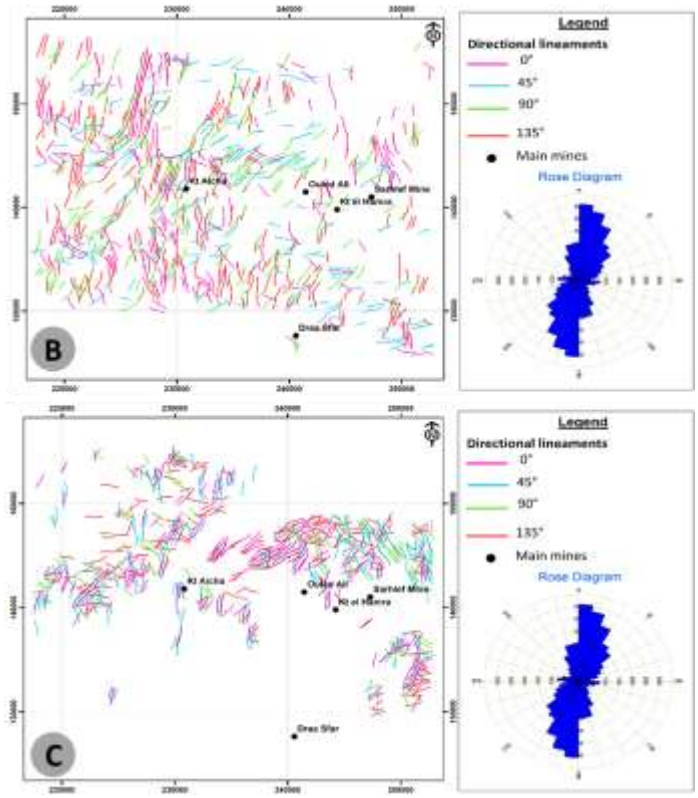

Fig. 8: (A) Map of the lineaments extracted using CP1 band, (B) Map of lineaments extracted using DEM

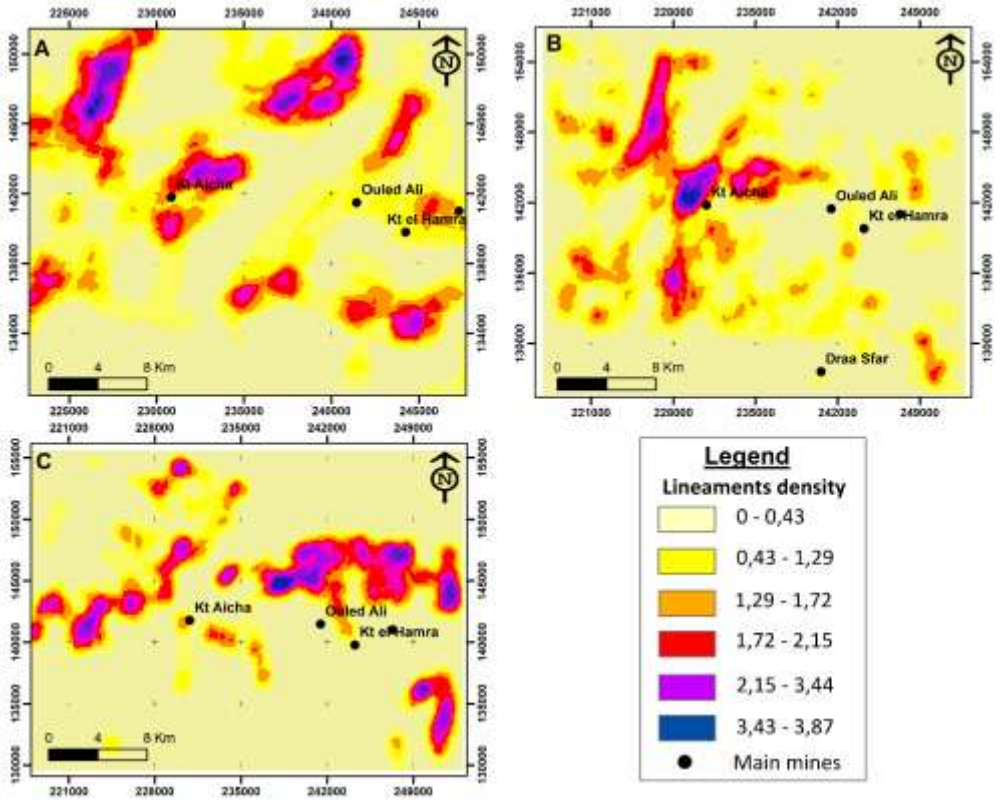

Fig. 9: Lineaments density maps of central jebilets, [(A) Geological map, (B) DEM map, (C) CP1map]

Mapping of mineral zones of hydrothermal alteration zones by ASTER spectral band treatments: This method is used to optimize spectral differences between bands (channels) and reduce the effect of shading caused by topography. It is based on the concept of reflectance and consists of dividing the digital number (DN) in one band by the DN of the corresponding pixel in another band. This technique is useful for the quantitative detection of hydrothermal alteration[8]. Several band reports have been proposed and verified for the detection of few minerals or groups of minerals associated with hydrothermal alteration[17]. The report (Band 4/Band 3), used to map iron oxide distribution, using this report on the ASTER image of our study area and shows high iron oxide contents. The report highlights the presence of minerals such as alunite, kaolinite and pyrophyllite, these minerals appear in dark pixels on the resulting greyscale image[18].

The ratio ((Band 7+ Band 9) / Band 8), highlights the presence of minerals such as carbonate, chlorite and epidote (Rowan,) and the ratio [(Band 6+ Band 9) / (Band 7+ Band 8)] for the endoskarns. The ratio ((Band 5+ Band 7) / Band 6) is characteristic of phyletic alteration by the presence of minerals such as sericite, muscovite, smectite and epidote (ROWAN USGS).

The maps in Figure 10 present the results of these reports after application of the masks to the vegetation areas extracted by the report (Band3 / Band2) and also to the current formations. Figure 10 also presents the results of the chlorite and sericite showings which appear to be very important under studying hydrothermal alteration of central jebilets (Board1 in appendices figures A, B, C, D and E).

Discussion

The ASTER images was used in this region and this study required a process of atmospheric, radiometric and reflectance corrections before being processed to produce the alteration mineral maps. The main treatments used are color compositions, band ratios, Principal Component Analysis (PCA), Minimum Noise Fraction (MNF) and Optimum Index Factor (OIF). These treatments allowed a good lithological discrimination, extraction maps of alteration minerals as shown in the earlier figures.

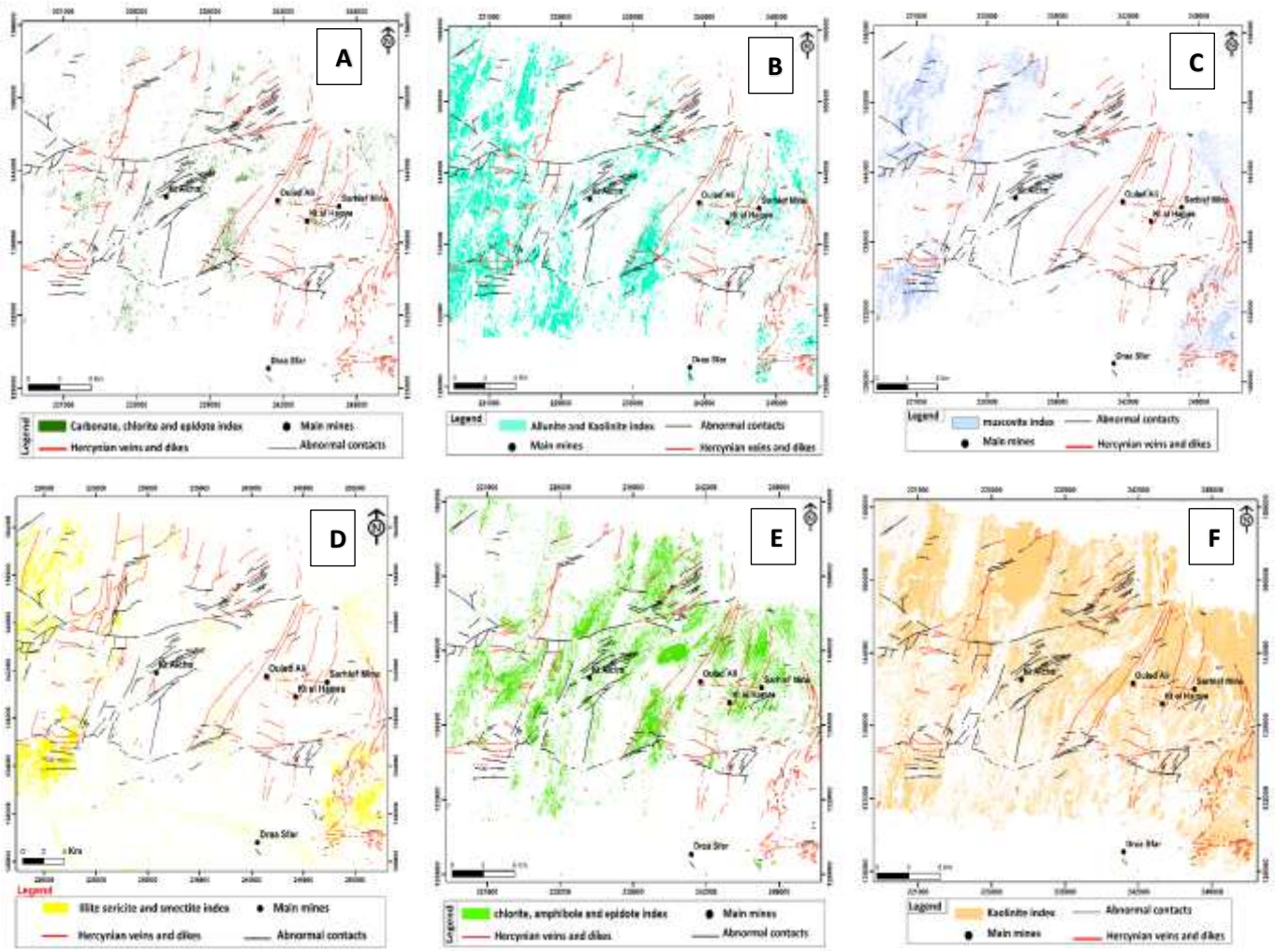

Fig. 10: Spatial maps of alteration mineral occurrences at the Central Jebilets. A. Chlorite, amphibole and epidote index, B. Kaolinite index, Muscovite index, D. Illite sericite and smectite index, E. chlorite Amphibole and epidote index, F. Kaolinite index.

The resulting band ratio image processing space maps shows a distribution of hydrothermal weathering minerals containing AL(OH) radicals such as Alunite, Muscovite, Kaolinite and Illite show characteristic absorptions in the region of the electromagnetic spectrum covered by these bands (2.14 µm - 2.28 µm). Chlorite and epidote are more abundant than sericite and illite. Iron oxides are highly concentrated in the central jebilets.

The superimposition of the geographical positions of the mines on the alteration maps shows a coincidence of the chlorite zones with a maximum of mines and showings. In perspective, a focus of the cartographic analysis of spectral signatures will be made at the level of the zones of maximum alteration of illite, chlorites and iron oxides in order to verify the cartographic zonation at a large scale. The field missions carried out made it possible to correctly validate the extracted information from the images and spatial maps (Figure 10).

Appendices

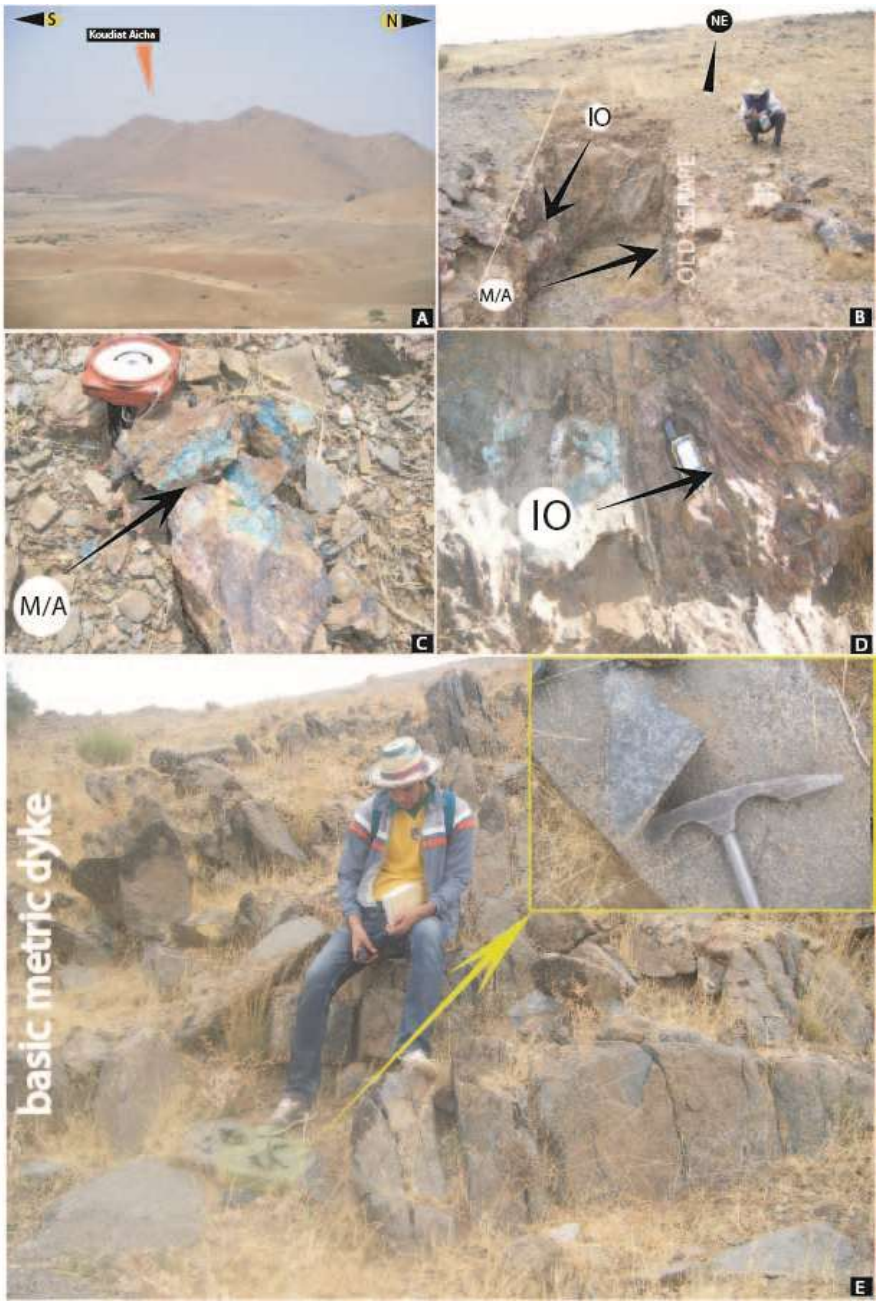

Board 1: Some photos taken on the study site, (A). photo showing a panoramic view of a hill in the central jebilets (Laachach North), (B). old mine scraping, (C) alteration minerals of copper (azurite in blue and malachite in green), collected in an iron cap with direction almost N20, (D) iron oxides (hematite and goethite), (E) basic metric dyke with quartz phenocrystals in metadolerites

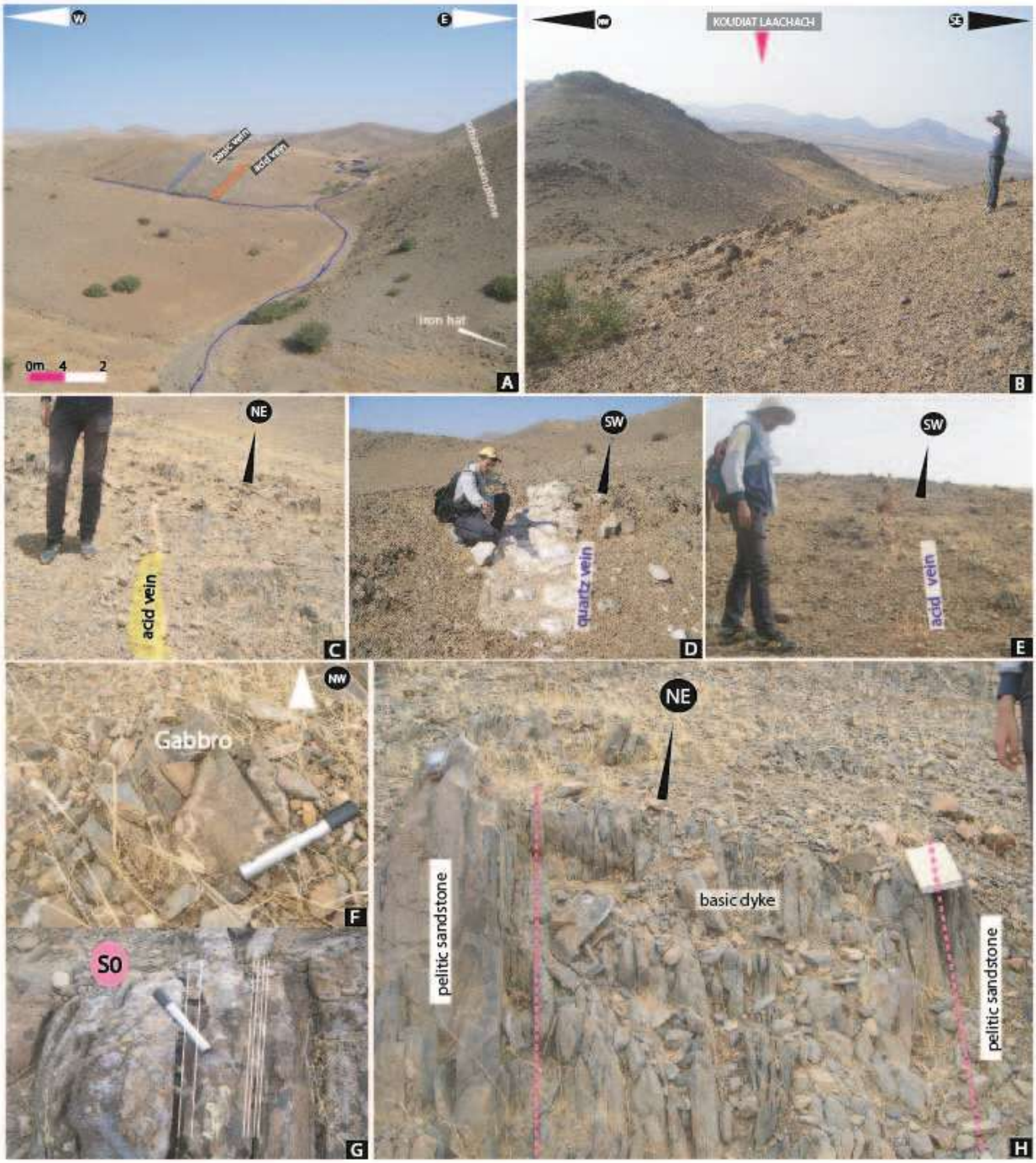

Board 2: Some photos taken on the study site, (A) panoramic view in a hill shows some geological elements such as basic and acidic dykes, iron cap, sedimentary host, (B) other panoramic view towards Marrakech, (C,E), Acidic micro dyke in NE direction,(D) filling of fractures with white quartz of SW direction,(F) gabbroic facies,(G) stratified sandstone,(H) basic dyke of NE direction, crosses the pelitic sandstone bedrock

Conclusion

The improvement techniques applied in this study, combined with previous field observations and lithological mapping studies of central jebilets are as the maps resulting from the ACP and MNF transformations have well discriminated between acidic and basic magmatism bodies, granodioritic plutons and large dioritic veins characterizing the high magmatic activity in the central jebilets. On the other hand, concerning the sedimentary volcano formations namely, the BMF treatment seems very strong to map limestones and metapelites of upper visian. A very good cartographic analysis of the central jebilet lineaments which generally consists of two families of direction faults, NE-SE and N-S, was obtained.

Furthermore, the cartographic analysis of spectral signatures shows the maximum alteration zones of the central jebilet alteration minerals (Figure 10) illite, chlorite and iron oxide in order to verify the large-scale cartographic zoning. The

field missions carried out enabled the information extracted from the images and spatial maps to be properly validated.

Acknowledgement

We would like to thank the Faculty of Sciences Semlalia Marrakech (FSSM) and also the Centre d'Analyse et de Caractérisation (CAC) for the support that allowed us to overcome some technical problems encountered during the map processing and the interpretation as well.

References

1. Aarab El., Genèse et différentiation d'un magma tholeitique en domaine extensif intracontinental : l'exemple du magmatisme pré-orogénique des Jebilet (Maroc Hercynien), Thèse Doctorat d'Etat, Univ. Caddi Ayyad, Marrakech **(1995)**

2. ASTER N., Advanced spaceborne thermal emission and reflection radiometer, Disponible **(2004)**

3. Belkabir A., Gibson H., Marcoux E., Lentz D. and Rziki S., Geology and Wall-Rock Alteration at the Hercynian Draa Sfar Zn-Pb-Cu deposit, Morocco, *Ore Geology Reviews*, **33**, 280-306 **(2008)**

4. Ben Aissi L., Contribution à l'étude gîtologique des amas sulfurés polymétalliques de Draa Sfar et de Koudiat Aïcha : comparaison avec les gisements de Ben Sliman et de Kettara (Jebilets centrales, Maroc hercynien), Thèse de doctorat, Uni Cadi Ayyad, Marrakech, 333 **(2008)**

5. Bordonaro M., Tectonique et pétrographie du district à pyrrhotine de Kettara (Paléozoïque des Jebilet, Maroc), Thèse de 3ème cycle, Univ. Louis Pasteur de Strasbourg **(1983)**

6. Boardman J.W. and Kruse F.A., Automated spectral analysis: a geological example using AVIRIS data, north Grapevine Mountains, Nevada: in Proceedings, ERIM Tenth Thematic Conference on Geologic Remote Sensing. Environmental Research Institute of Michigan, *Ann Arbor*, **MI**, I-407-I-418 **(1994)**

7. Chavez P.S., Berlin G.L. and Sowers L.B., Statistical method for selecting landsat MSS, *J. Appl. Photogr. Eng*, **8(1),** 23-30 **(1982)**

8. Di Tommaso I. and Rubinstein N., Hydrothermal alteration mapping using ASTER data in the Infiernillo porphyry deposit, Argentina, *Ore Geology Reviews*, **32(1-2),** 275-290 **(2007)**

9. Essaifi A., Relation entre magmatisme-déformation et altération hydrothermale. L'exemple des Jebilet centrales (hercynien, Maroc), Thèse Doctorat d'Etat, Univ. Caddi Ayyad, Marrakech **(1995)**

10. Franklin J.M., Gibson H.L., Jonasson I.R. and Galley A.G., Volcanogenic massive sulphide deposits, *Economic Geology*, 523–560 **(2005)**

11. Hibti M., Les amas sulfurés des Guemassa et des Jebilet (Meseta Sud-Occidentale, Maroc) : Temoins de l'hydrothermalisme précoce dans le bassin mesetien, Thése de Doctorat d'Etat EsSciences, Unv. Marrakech, 301 **(2001)**

12. Huvelin P., Etude géologique et gîtologique du massif Hercynien des Jebilet (Maroc Occidental), Noteet Mém. Serv. Géol. Maroc, Rabat, N° 232 bis, 307 **(1977)**

13. Gaillet J.L. and Bordonaro M., La tectogenèse hercynienne dans le massif Dinantien des Jebilet centrales (Maroc), *Sciences Géologiques, Bulletins et Mémoires*, **34(2),** 117-122 **(1981)**

14. Kalinowski S.T., Counting alleles with rarefaction: private alleles and hierarchical sampling designs, *Conservation Genetics*, **5(4),** 539-543 **(2004)**

15. Moreno C., Sáez R., González F., Almodóvar G., Toscano M., Playford G., Alansari A., Rziki S. and Bajddi A., Age and depositional environment of the Draa Sfar massive sulfide deposit, Morocco, Miner Deposita, DOI 10.1007/s00126-008-0199-x **(2008)**

16. Piqué A. and Michard A., Les zones structurales du Maroc hercynien, *Sciences Géologiques, Bulletins et Mémoires*, **34(2),** 135-146 **(1981)**

17. Richards J.A. and Richards J.A., Remote sensing digital image analysis, Berlin et al, Springer, 10-38 **(1999)**

18. Rouskov K., Popov K., Stoykov S. and Yamaguchi Y., Some applications of the remote sensing in geology by using of ASTER images, In Scientific Conf. "SPACE, ECOLOGY, SAFETY" with Int. Participation, 167-173 **(2005)**.

(Received 06th July 2020, accepted 11th September 2020)